

High-resolution ground verification, cluster analysis and optical model of reef substrate coverage on Landsat TM imagery (Red Sea, Egypt)

S. PURKIS*, J. A. M. KENTER,

Department of Earth Sciences, Vrije Universiteit, De Boelelaan 1085, 1081 HV Amsterdam, The Netherlands

E. K. OIKONOMOU and I. S. ROBINSON

Department of Oceanography, Southampton University, Southampton Oceanography Centre, European Way, Southampton SO14 3ZH, UK

(Received 28 September 1998; in final form 28 June 2000)

Abstract. A combination of high-resolution ground verification, cluster analysis using Landsat Thematic Mapper (TM) data, and optical modelling was applied to Red Sea reef substrate. Ground verification, in an area of 3 by 20 pixels (90 by 600 m) with one metre scale resolution, identified the presence of 30 different bottom types that were later reduced to twelve dominant bottom types. A combination of bispectral plots and principal component analysis using spectral bands 1, 2 and 3 confirmed the presence of nine bottom types. The identified clusters were separated and used as a training set to classify substrate. Optical modelling, using literature radiance values and coverage of the original twelve dominant bottom types and a simple model for atmospheric and water column absorption, revealed a difference of up to 60 W m^{-2} between predicted substrate radiance and the satellite sensor values in the reef top area. Considering the simple atmospheric correction model, the lack of *in situ* radiance measurements and the uncertainties with respect to possible changes in bottom type distribution since the acquisition of the 14 year old image, the results show the potential use of satellite imagery for reef research in both biological and geological analysis through very precise and semi-quantitative ground verification, including *in situ* reflectance measurements.

1. Introduction

Coral reefs and the associated carbonate shelves have been mapped and surveyed repeatedly for over 150 years. Reefs and associated sediments are an important element in the carbon cycle. The 'reef hypothesis' of Quaternary climate change attributes part of the increase in atmospheric CO_2 during deglaciations to extensive fixation of marine calcium carbonate by reef growth during a transgression (Berger 1982, Milliman and Droxler 1996). In addition, these systems are highly specialized and complex ecosystems that respond to changes in the environment. Of particular concern is change by global warming (Glynn 1991) and by eutrophication from agricultural fertiliser and sewage—a serious problem for island nations depending

*e-mail: purs@geo.vu.nl

on reef fishery and coastal-plain agriculture (Hallock and Schlager 1986, Grigg and Dollar 1990). Finally, reefs and associated sediments are highly porous and host nearly one half of the world's reserves of hydrocarbons and contain some of the largest aquifers on Earth.

The introduction of remote sensing has provided information more efficiently and at lower cost than conventional techniques in some application areas. Remote sensing has been used for more than two decades in reef studies, particularly in the context of regional documentation and reef monitoring for the preservation and sustainable development of reefs (e.g. Smith 1975, Manière and Jaubert 1985, Kuchler *et al.* 1986, Luckovich *et al.* 1993, Peddle *et al.* 1995, Maritorea 1996, Maritorea and Guillocheau 1996, Matsunaga and Kayanne 1997, Borstad *et al.* 1997a, b). Although these published studies on coral reefs and associated sediments were only partly successful in separating bottom types, they demonstrated the potential for reef research and have shown that satellite imagery can provide quantitative, standardized data that may play a pivotal role in both biological and geological analysis.

This paper presents the results of a comparative study of Landsat TM imagery and ground verification of a Red Sea fringing reef system. The reefs of the Red Sea constitute a 27 000 km² area which represents 4% of the world's total reef area. A brief description of the various bottom types was presented by Riegel and Piller (1997). The coastline south of Hurghada to the Sudanese border is characterized by fringing reefs with inlets, bays, offshore patch reefs and island reefs. South of Safaga down to Ras Banas there is continuous, often well-developed fringing reef but the continental shelf in this area is narrow and the seabed falls away rapidly preventing the formation of offshore reefs. *In situ* data were collected 111 km and 113 km south of the port of Quseir on the Egyptian Red Sea coast (figure 1). High-resolution maps of the reef substrate were made and used to derive the distribution of dominant bottom types on the reef top. This bottom type map was successfully calibrated with the radiance values of the satellite image through cluster analysis. The resulting training set was used for supervised classification of the satellite pixels. Finally, the crude foundations for an optical model to simulate reef substrate radiance values in the study area are presented. In the absence of *in situ* measurements with a portable spectroradiometer and a dedicated library of accepted spectral signatures of reef substrates collected under standardized conditions, the model was developed using literature derived radiance values. The modelled radiance values were compared to those of the normalized Landsat TM image and differences of up to 60 W m⁻² were observed.

2. Methodology and results

An inventory of morphology and living conditions of reefs and related sediments on pixel-scale through ground verification, cluster analysis and optical modelling required the following steps: (1) georeferencing of the satellite image and the subsequent location of the study area within it; (2) high-precision ground verification; (3) cluster analysis using bispectral and principle component analysis; (4) development of an optical model to simulate the radiance of key bottom types, including corrections for atmospheric absorption, solar elevation angle and water attenuation.

2.1. Study area and image matching

The study area is within scene ID list LT5173043008421110, acquired 29 July 1984. The limited budget allocated for the study dictated that only vintage (10-year

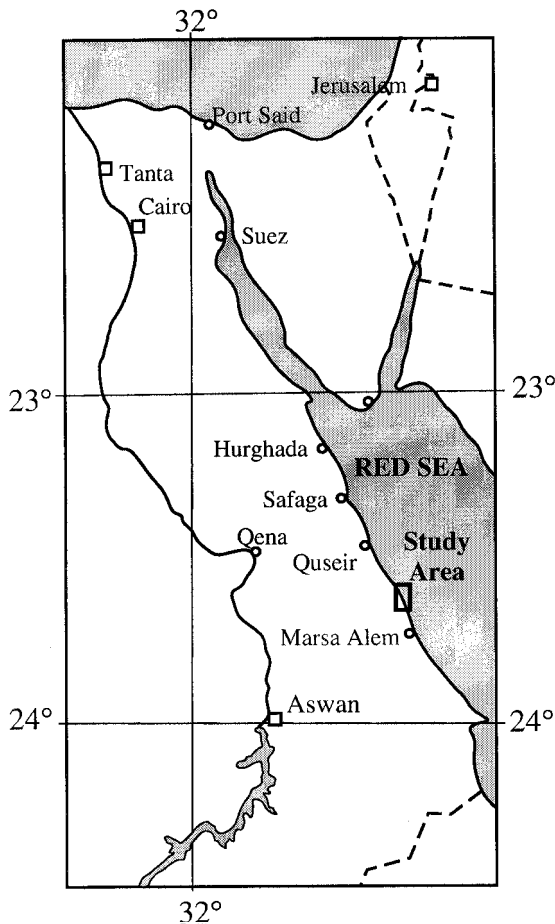


Figure 1. A simplified map of the Egyptian Red Sea, with the study area shown on the coast.

and older) images could be purchased. It was accepted that during the fourteen years that had elapsed between the satellite overpass and the completion of the fieldwork, there may have been changes in the reef substrate and therefore we could have been ground verifying a different ecosystem than the satellite data recorded. It was realized that this lag time between satellite overpass and the ground verification exercise may be a dominant factor influencing the comparison of the data sets. In general, a pattern of shore-parallel banding on the TM image along the Red Sea coast is visible (figure 2B and C). The study area was selected for the extended width of these bands as well as for the ease of access to the reef top from the base camp.

Following the selection of the ground study pixels, Global Positioning System (GPS) measurements were used to georeference the satellite image and to identify the study pixels that were mapped on the ground in an area of 3 by 20 pixels (90 by 600 m) with a metre scale resolution. GPS measurements of nine control points (three road junctions and six prominent headlands on the coast in close proximity to the study area) were recorded for a period of 90 min, which should assure an accuracy of 2 m (Leavitt and Payton 1996). Simple mathematics were used to identify the pixels on the satellite image using the latitude and longitude values of the image

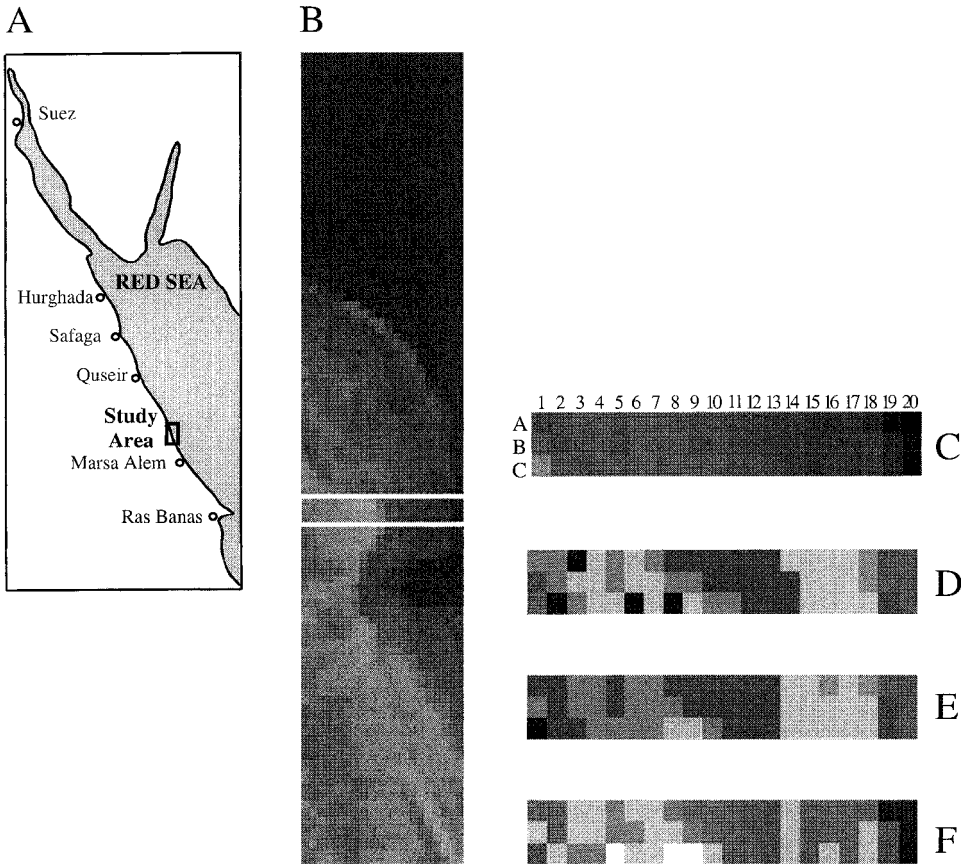


Figure 2. (A) Map showing study area. (B) Grey shaded 20 by 101 pixels Landsat TM image (bands 1, 2 and 3) equivalent to the study area in (A); the highlighted box represents the ground-truthed pixels. (C, D, E, F) Grey shaded 20 by 3 pixels Landsat TM image of composite and separate bands 1, 2 and 3 respectively, corresponding to the pixels highlighted in (B).

extent as extracted from its header file as reference points with which to convert latitude and longitude to pixel X and Y co-ordinates. The predicted pixel co-ordinates of the nine control points were shown to have a small common offset, which was added to the derived pixel X and Y co-ordinates, the result being that the ground control points identified in the field could now be identified on the image. The image was also rectified to a Universal Transverse Mercator (UTM) projection of the US Geological Survey (USGS) zone 36. The UTM co-ordinates of the four corners and the centre point of the image were taken from the header file and entered along with the nine control points recorded in the field, into the desktop image processing software, ER Mapper 6.0. The maximum root-mean error (RME) was calculated to be 15.39 m. The resulting rectified image was used to re-confirm the accurate positioning of the *in situ* ground-truthed study area. Following standard routines (e.g. Richards 1986), the DN (digital number) values of bands 1, 2 and 3 were converted to radiance. The transformation is based on a calibration curve of DN to radiance, which has been calculated by the operators of the satellite system. The calibration

concerns the bias and gain of the sensor, the gain represents the gradient of the calibration and the bias defines the spectral radiance of the sensor for a DN of zero. Bias and gain values for each band are supplied with the image and take into account when the image was processed, as the accuracy of the satellite declines as the sensitivity of the sensor changes over time. The calibration is given by the following expression for 'at-sensor' spectral radiance, $L_i \text{ W m}^{-2} \text{ str}^{-1} \mu\text{m}^{-1}$ (for Landsat).

$$L_i = \text{Bias} + (\text{Gain} \times \text{DN}) \quad (1)$$

The converted radiance values for the pixels corresponding to the ground-truth area are plotted using a grey scale in figures 2C, D, E and F. Archive tidal data for the area was obtained from Nautical Software Inc. (Beaverton, Oregon) and used to determine that on 29 July 1984 at 09:36 local time, the depth was 0.58 m above low water datum. Repeated measurements at the study site using a graduated pole identified the position of the low water datum on the reef. The submergence depth of the reef top at the time of the satellite overpass could then be calculated by combining the *in situ* measurements and the archive tidal data.

2.2. Ground verification

In situ data were collected on a $600 \text{ m} \times 90 \text{ m}$ section (3×20 Landsat TM pixels) of coral reef top between the shoreline and the reef crest (fig 2B). A rope quadrant ($15 \text{ m} \times 15 \text{ m}$) was used which was moved along the pre-determined transect and matched to the pixel columns of the satellite image (figure 3).

The various bottom types of the reef top were mapped using $5 \text{ m} \times 5 \text{ m}$ rope subdivisions of the main quadrant. A plastic slate with a ready prepared pixel grid and a list of recognized bottom types was carried by each mapper and the substrate boundaries were drawn onto the slate and labelled; this process was continued over the reef crest to 25 m water depth using SCUBA diving equipment. To ensure that accurate mapping of the reef had been carried out, several pixels were re-visited and re-mapped.



Figure 3. Photograph of the bottom types being mapped on the reef top using the rope quadrant.

Primary criteria for discriminating between bottom types were type and percent coverage of red, green and brown algae, seagrass or coral on the background of mostly mixed and fine-grained carbonate sand. Initial mapping of the reef top *in situ* yielded 30 distinct bottom types (figures 4A–B and 5A–F). Data reduction was accomplished following two criteria. First, the groups were formed by similar dominant spectral response based on previous works (Armstrong 1993, Zainal *et al.* 1993, Maritorea *et al.* 1994). Second, the bottom types were combined based on their association with neighbouring groups. As a result, twelve dominant bottom types remained (figure 4B and table 1). Next, the percentage of each of the twelve bottom types present in each pixel was calculated via standard image analysis techniques using the geographic data processing software, Idrisi 2.00.

2.3. Cluster analysis and supervised classification

Since the presence of water on the reef top, which absorbs near infra red light, dominates the signatures in bands 4 to 7, only the first 3 bands (i.e. blue, green and red) were considered in the analysis that follows. As the fieldwork took place prior to imagery analysis, the determination of the number of bottom classes mapped on the reef is independent of the apparent classes on the image. The analysis in this way contains an element of supervised classification because ground measurements are used to classify the image, but also unsupervised classification as the bottom type classes derived from the field survey do not necessarily relate to the classes identified on the imagery. To reveal relationships between bottom types and radiance, bispectral plots as well as principle component analysis (PCA) was applied.

Provided that there was good discrimination between the spectral bands, it was expected that the pixels would form groups corresponding to different bottom types, the size and shape of these groups depending upon the density of cover type, systematic noise and bathymetric effects. Bispectral plots of the radiance values revealed relationships in multispectral space including clustering of bottom types and the effects of bathymetry (figures 6A and 6B).

PCA has been used effectively in many studies as a data reduction technique and as a means to identify modes of data. PCA, in conjunction with other techniques was used by Holden and LeDrew (1997) to make a spectral discrimination of bleached and healthy submerged coals. The principal components analysis indicated that 97% of the variance of the three bands occurs along the first PC axis, with negligible variance along axes two and three. By plotting the PCs of the second and third axis against the first, the clustering of pixel points was obtained (figures 6C and 6D). The principal components yielded the same number of clusters as the bispectral plots but their association differs in two cases, implying that bispectral and PCA plots have a similar capacity for resolving clusters of pixels.

Initially twelve bottom type classes were identified during the survey (table 1) and the data were analysed to give the percentage cover of each of the coverage classes. The purest pixel on the image associated with one of these classes was then geolocated and isolated. The radiance and PC ordinates of the pure pixels were then estimated in both bispectral and PCA plots. In order to distinguish the pure pixels they were re-plotted with a diamond symbol (figure 6). The majority of the previously defined clusters became associated with a pure pixel end-member, and thus they could be classified. With the addition of the pure end-members to the plots the clusters were re-defined by resolving digitally the maximum and minimum band 1 (x-axis) and band 2 or 3 (y-axis) values in the bispectral plots. The boundary

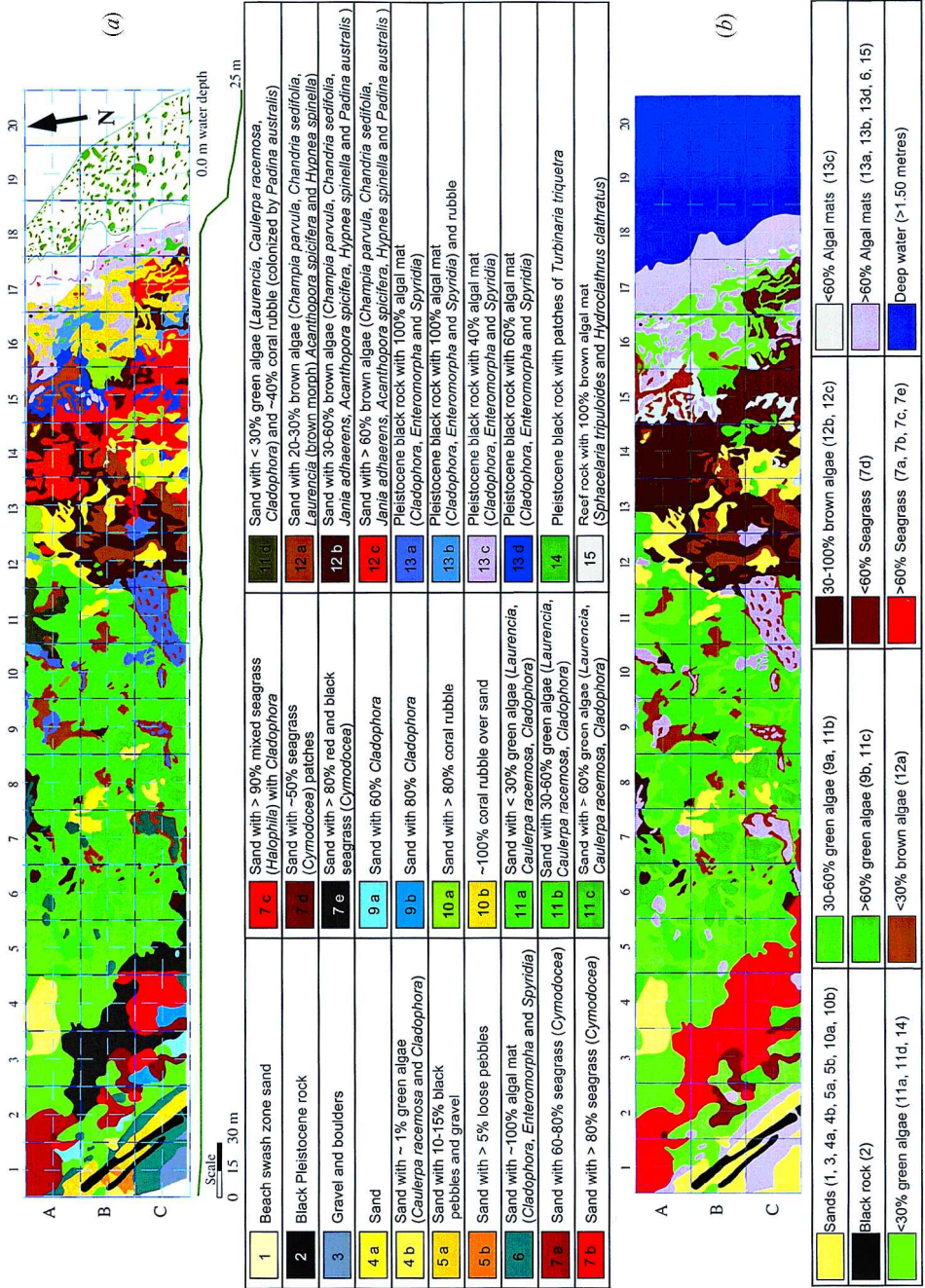


Figure 4. (a) Key substrate types discriminated in the 20 by 3 ground pixel (approximately 600 by 90m) study area. In this initial approach 30 categories of bottom type were identified. (b) Simplified map with only 12 remaining categories (see table 1).

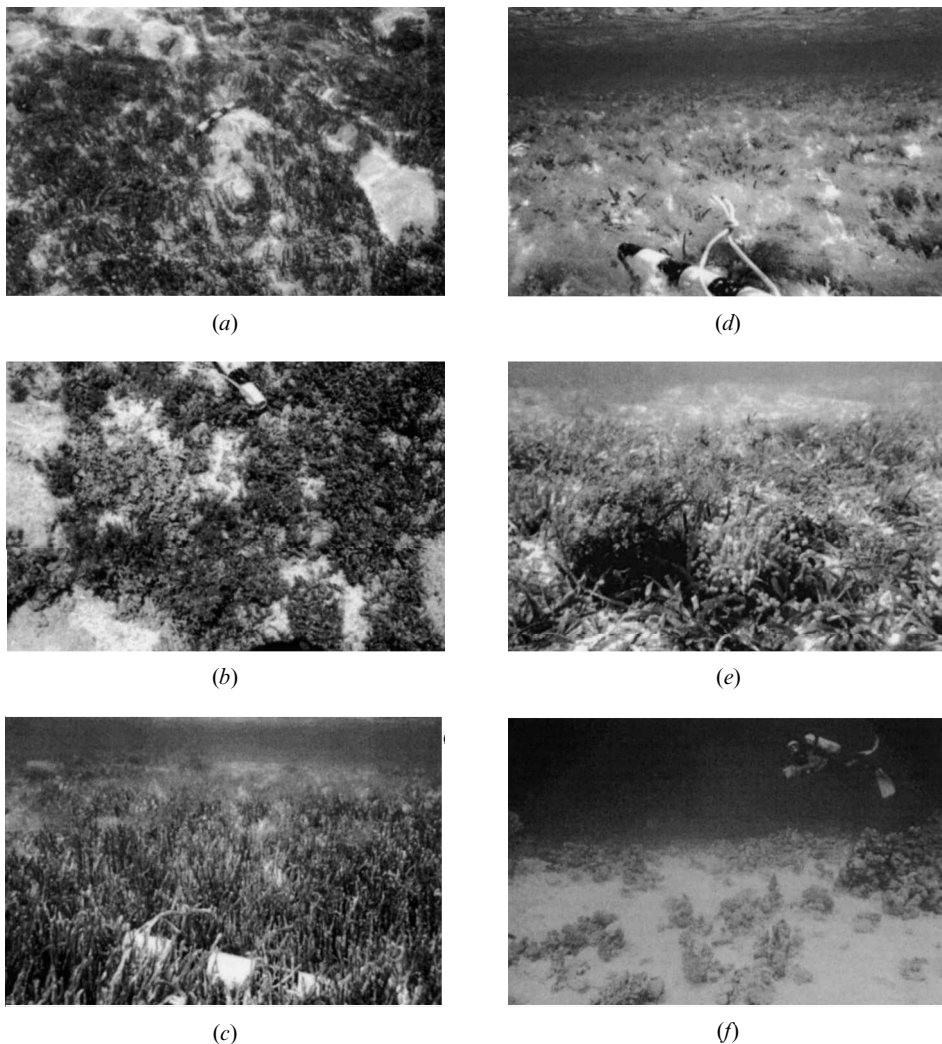


Figure 5. Photographs showing examples of initial substrate coverage categories. Background is mixed siliciclastic and carbonate sand. (a) *Laurencia* type assemblage of green algae; less than 30% in plan view. (b) Approximately 60% *Champia parvula*. (c) *Caulerpa racemosa*; more than 80% in plan view. (d) Between 30% and 50% coverage of *Cladophora*. (e) Between 60% and 80% coverage by *Cymodocea* seagrass. (f) Carbonate sand with less than 10% coral coverage in 22 m of water.

co-ordinates of each cluster were modified to list all pixel co-ordinates which lay within the limits. When clusters in close proximity to each other were found to have common pixels, the cluster boundaries were re-defined until no pixels were common to more than one group. All the clusters were then allocated an identification code and were defined according to the origin of the pure pixel end-member with which they seem to be associated. Those clusters not related to any pure pixel were considered unclassified (see table 2).

The bispectral plots of band 1 against band 2 (referred to as B2-1) and band 1 against band 3 (referred to as B3-1) show a clear distinction of the deep water cluster

Table 1. The 12 dominant bottom types recorded during *in situ* ground verification.

No.	Class of ground truth
1	Sand
2	Black rock
3	<30% Green algae
4	30–60% Green algae
5	>60% Green algae
6	<30% Brown algae
7	30–100% Brown algae
8	Seagrass <60%
9	Seagrass >60%
10	Algal mats <60%
11	Algal mats >60%
12	Deep water

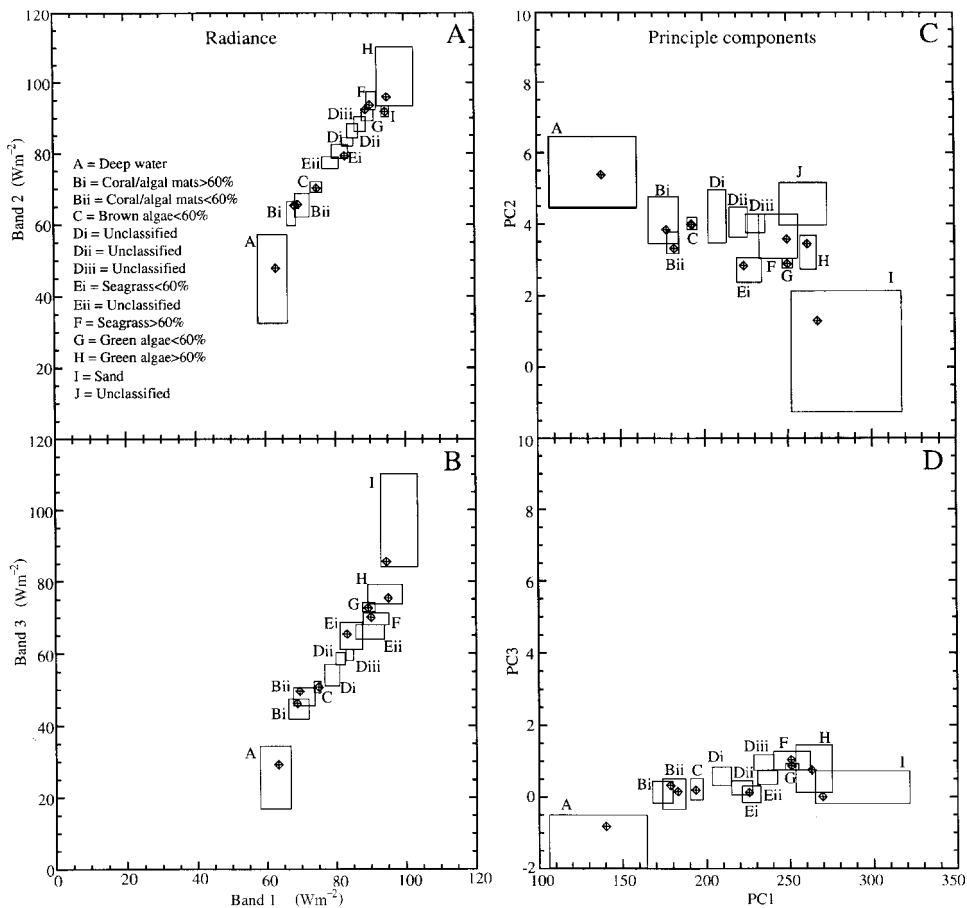


Figure 6. (A) Bispectral plot of radiance in TM band 2 versus band 1. (B) Bispectral plot of radiance in TM band 3 versus band 1. (C) Scatter plot of PC 3 versus PC 1. (D) Scatter plot of PC 3 versus PC 1. The boxes represent the maximum and minimum values of the pixels in each cluster.

Table 2. The 14 clusters identified by bispectral plots and PCA, and their classification after the addition of pure pixels from the ground verification.

No.	Cluster classification	Cluster identification code
1	Deep water	A
2	Coral/algal mats >60%	Bi
3	Coral/algal mats <60%	Bii
4	Brown algae <60%	C
5	Unclassified	Di
6	Unclassified	Dii
7	Unclassified	Diii
8	Seagrass <60%	Ei
9	Unclassified	Eii
10	Seagrass >60%	F
11	Green algae <60%	G
12	Green algae >60%	H
13	Sand	I
14	Unclassified	J

(figure 6A and B). The separation is optimum in B3-1, which also separates most effectively the two densities of coral with algal mats. B2-1 exhibits the tightest clustering of the three unclassified groups D(i), (ii) and (iii), although distinction between them is easier in B3-1. Both band plots resolve seagrass <60% into an end-member classified group situated between four unclassified groups. The splitting of the seagrass >60% and green algae <60% is best in B3-1, however, not to the extent offered by the principal components plot of PC3-1 (figure 6D). The position of the sand cluster in B2-1 is unique in the sense that it is not at the extreme end of the clusters, but instead it is located between two clusters of green algae and one of seagrass (clusters F, G and H respectively). Clearer definition between sand and chlorophyll containing substrate is offered with the bispectral plot of B3-1 than with B2-1 as the responses in the red–blue portion of the visible spectrum are being considered. Chlorophyll predominantly absorbs energy of the red portion of the spectrum and has a reflectance maximum in the green, therefore the bispectral plot that contains information from TM band 3 (i.e. B3-1) should give improved discrimination between chlorophyll and non-chlorophyll containing substrates, than a plot of B2-1 (wavelengths corresponding to the green portion of the spectrum against blue). This explains the more distinct discrimination between sand, and the algal and seagrass clusters using plot B3-1, than with B2-1.

PCA provides a method for confirming the interpretation of the radiance made above. The main result of PCA is that one extra cluster has been revealed which was not recognizable in the bispectral plots. As with the bispectral plots, the PCA graphs (figure 6C and D) give excellent discrimination of deep water, as well as between the unclassified groups D(i), (ii) and (iii). The plot of PC2-1 provides the clearest distinction between the two coral with algal mat densities and is unique in only resolving the classified E(i) cluster group (i.e. seagrass <60%) but with the unclassified E(ii) being absent. Despite this omission, the PC2-1 plot is characterized by the description of the extra unclassified group J not observed in the PC3-1 graph. The fact that a new cluster has been resolved via the application of PCA confirms that the technique is valuable if maximum information is to be drawn from the data set. Both PCA plots give a clear separation of the cluster group associated with

sand. Additionally PCA further facilitates the distinction of pixels containing coral with algal mats or brown algae.

Since the boundaries of the nine ground verified clusters were now defined in terms of their radiance values in the first three bands, the satellite pixels were classified using bispectral plots and PCA (figures 7B and C respectively). The satellite pixels were then re-classified using only the six major classes of bottom type for the bispectral plots and PCA (figures 7D and E respectively).

Both 'supervised' classification models show a clear zonation of bottom types that are easily identified on the simplified substrate map with twelve dominant group types (figure 4B). Clearly, un-identified mixtures of bottom types were not used in this classification. There are slight differences in the results of classifying the satellite pixels of the study area using the cluster limits defined by the bispectral and PCA plots. The differences in most cases, are revealed to be related to variations in the classification between pixels of the same substrate but at different concentrations. When the nine substrate types recognized using the bispectral and PCA plots are reduced to six types by grouping substrates at different densities into a single heading, the classifications become more similar (figures 7D and E). Classification using the PCA plots gives three pixels dominated by sand, whereas with the bispectral data, only one is revealed. The mid section of the reef is classified in both cases as being composed of green algae and seagrass, although the bispectral data shows the occurrence of green algae to be higher, and beyond pixel row 14 classification is identical.

2.4. Optical model

With the field data of the northern reef top transect having already been broken down from 30 bottom type categories to a more manageable twelve (figure 4), a prediction of their spectral signatures could be made for comparison with the Landsat imagery. A hand-held spectroradiometer that could measure the spectral response of bottom types in each of the TM bands was not available at the time of the fieldwork. Instead, by combining the spectral measurements carried out by Maritorena *et al.* (1994) in French Polynesia with those of Armstrong (1993) in the Bahamas, representative spectral characteristics of sand, green algae, brown algae and seagrass could be applied to the fieldwork of the Red Sea. Maritorena *et al.* (1994) used a LiCor LI-1800 UW spectroradiometer (spectral resolution ~ 8 nm) to measure the upwelling radiance of various bottom substrates within the Takapoto atoll of French Polynesia. Sites of the homogeneous bottom cover were selected, within the proximity of the deep zone. The data collected by Maritorena *et al.* were considered the most appropriate to be applied to the data collected in the Red Sea study, as the measurements were made on cloud-free days with calm seas under high solar elevation. These criteria are equivalent to the prevailing conditions of the Red Sea during July (month of satellite overpass). Six reef substrates were measured, with an appropriate correction to account for any air-water interface reflection; coral sand, the green algae *Boodlea*, the two brown algae's *Sargassum* and *Turbinaria* and the two red encrusting algae's *P. ankodes* and *Corallinacea*.

The study of Maritorena *et al.* (1994) did not provide information on the upwelling radiance of seagrass. An estimate for the spectral response of seagrass was taken from work carried out near Lee Stocking Island in the Bahamas by Armstrong (1993). Unlike the work in French Polynesia, Armstrong (1993) did not make spectral measurements *in situ* but instead collected samples and processed them later in the

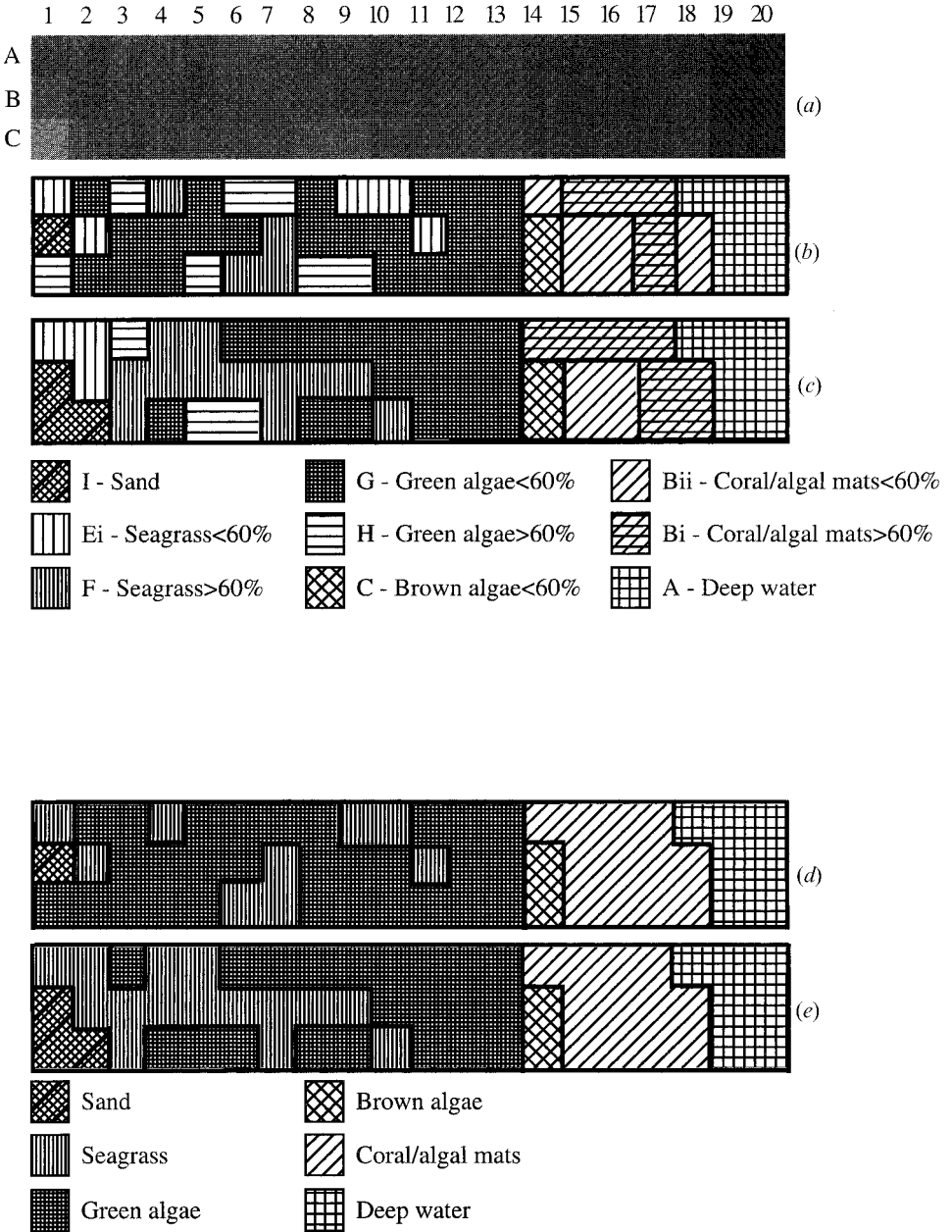


Figure 7. (a) Grey shaded 20 by 3 pixels Landsat TM image of composite bands 1, 2 and 3. (b) Classified substrate map for the 20 by 3 pixel study area using cluster dimensions from bispectral plots. (c) Classified substrate map for the 20 by 3 pixel study area using cluster dimensions from PCA plots. (d) Classified substrate map for the 20 by 3 pixel study area using cluster dimensions from bispectral plots further reduced to the six major substrate types. (e) Classified substrate map for the 20 by 3 pixel study area using cluster dimensions from PCA plots further reduced to the six major substrate types.

day using a Spectron SE590 spectroradiometer with an integrating sphere. It is appreciated that too many assumptions were taken by using spectral measurements acquired from different geographical areas, without corrections being applied to compensate for the differing atmospheric and solar geometry conditions, using equipment with dissimilar spectral bandwidths and radiometric resolutions, to make a viable comparison of actual radiance values. The object of the exercise was not to create a fully functioning optical model with which to simulate the true spectral signatures of reef substrates in the Red Sea. Instead, the exercise was considered as a preliminary study with which to assess the value of a second phase of fieldwork during which actual radiance values of reef substrates would be collected *in situ* using a portable visible and near infrared spectrometer.

By combining the spectral measurements carried out by Maritorena *et al.* (1994) in French Polynesia with those of Armstrong (1993) in the Bahamas, representative spectral characteristics of sand, green algae, brown algae and seagrass could be applied to the field work of the Red Sea. Spectral signatures for the algal mats which are characteristic of the outer limits of Red Sea reefs and the black beach rock which divides the beach from the reef top could not be found in the literature. The beach rock only contributes to three pixels of the total area studied, and was presumed to give low radiance values in the visible TM bands. The algal mats on the reef top were predominantly brown in colour and so were considered to have a similar spectral response to that of brown algae.

The spectral signatures recorded by Armstrong (1993) and Maritorena *et al.* (1994) were used to estimate the expected radiance values for sand, green and brown algae and seagrass in TM bands 1, 2 and 3 (table 3).

With estimated percentage reflectance values for sand, green and brown algae and seagrass, the literature data could be used to estimate radiance values for the twelve bottom categories identified in the fieldwork. This was carried out by estimating the composition of the field classes in terms of proportions of the literature derived radiance measurements. Having deduced estimates of the spectral signatures for each of the twelve field categories, a model of hypothetical radiance values in the first three TM bands was generated (table 4).

In order to compare the satellite radiance values to those of the optical model the satellite image was normalized by applying corrections for the following effects: atmospheric scattering, solar elevation angle, and water attenuation (table 5). A simple method of atmospheric compensation in multispectral data is to observe the radiance recorded over target areas of essentially zero reflectance, e.g. far out at sea. Any signal observed in such an area represents the additive path radiance and, in this case, this value (average of 20 selected pixels) was subtracted from all pixels in that band of the satellite image to remove scattering effects. Using such a method

Table 3. Estimated radiance values ($W m^{-2}$) of bottom substrates derived from measurements by Armstrong (1993) and Maritorena *et al.* (1994) in Landsat TM bands 1–3.

Substrate	Band 1	Band 2	Band 3	Source
Sand	37.7	49	57	Maritorena <i>et al.</i> (1994)
Green algae	11.3	24	12.8	Maritorena <i>et al.</i> (1994)
Brown algae	3.7	10.2	7.3	Maritorena <i>et al.</i> (1994)
Seagrass	5	12.6	7.7	Armstrong (1993)

Table 4. Estimated radiance values (W m^{-2}) for the 12 bottom type categories identified in the fieldwork, using measurements by Maritorena *et al.* (1994) and Armstrong (1993).

No.	Class of ground truth	Band 1	Band 2	Band 3
1	Sand	38	49	57
2	Black rock	0	0	0
3	< 30% Green algae	30	42	44
4	30–60% Green algae	22	34	30
5	> 60% Green algae	11	24	13
6	< 30% Brown algae	28	37	42
7	30–60% Brown algae	19	26	27
8	Seagrass < 60%	18	42	27
9	Seagrass > 60%	5	13	8
10	Coral/algal mats < 60%	10	21	12
11	Coral/algal mats > 60%	5	13	8
12	Deep water	0	0	0

Table 5. Corrections for water column and atmospheric effects for the first three Landsat TM bands.

Landsat TM band	Wavelength (nm)	Range k_i (m^{-1}) literature sea water	Mean k_i (m^{-1})	Atmospheric scattering correction (W m^{-2})
1 Blue	450–520	0.01–0.03	0.02	54.14
2 Green	520–600	0.07–0.1	0.085	30.40
3 Red	630–690	0.45–0.78	0.62	20.16

for atmospheric correction does not take into account any inhomogeneity of the atmosphere that may exist over the image. Since at this stage we are only concerned with a very limited section of the image that relates to the study area, it was deemed that a simple atmospheric correction was sufficient. A more powerful correction would be employed if the method were to be expanded to model larger areas of reef, though this is out of the scope of this paper.

The Sun elevation correction accounts for the seasonal position of the Sun relative to the Earth. The Sun elevation angle at the time the Landsat TM image was acquired was 60.22° . To convert the Landsat TM pixel elements to a similar solar illumination angle we use the following equation:

$$E_2 = E_1 / \sin \theta_0 \quad (2)$$

where θ_0 is the solar elevation angle, E_1 is the uncorrected digital number of each pixel element, and E_2 is the corrected radiance value of each pixel element. The solar elevation angle is 60.22° . An Earth–Sun distance correction to normalize for seasonal changes in the distance between the Earth and the Sun was not applied here as no *in situ* spectroradiometric measurements were made.

A simple but effective model of light absorption by water is given by:

$$E_3 = E_2 - e^{-2kz} \quad (3)$$

where E_3 = digital number in band i that would be recorded from the wet sea bottom if there were no water overlying it; E_2 = digital value recorded for a picture element in band i ; k = absorption coefficient of water in band i ; z = water depth.

The only unknown is E_3 as values for the absorption coefficient for the different

wavelengths, k_i , for clear tropical water were taken from the literature, E_2 are the digital numbers from the satellite image, and z is known. Various authors have published absorption coefficients for clear tropical water; see, e.g., Maul (1985), Shifrin (1988), Spinrad *et al.* (1994), and Maritorena and Guillocheau (1996). Water column absorption has a negative effect on the synthetic digital numbers. The difference between the radiance values of the data modelled using literature spectral measurements and percentage cover of each of the twelve coverage classes, and those of the normalized satellite image were plotted as a series of graphs for each pixel row across the reef top for the first three Landsat TM bands (figures 8A, B and C respectively).

The graphs reveal differences between 0 and 60 W m^{-2} . In the shallow reef top area, differences are of the order of 10 to 20 W m^{-2} for band 1 and 20 to 30 W m^{-2} for bands 2 and 3. The pixels closest to the division between the exposed beach and the start of the submerged reef top show the greatest differences in radiance values (20 to 60 W m^{-2}). The large discrepancy between the modelled and normalized values in this area can be attributed to the fact that this section of the reef is dominated by mixtures of black Pleistocene beach rock, pebbles and brown algal mats. The literature only provided estimates of radiance values for brown algae, and so the modelled data were calculated assuming that this area was completely covered by this bottom type. Such examples highlight the need for either *in situ* measurements of radiance, or the development of a spectral library of reef substrate spectral signatures, if the model is going to be further developed. In contrast, the deeper water zone reveals small differences in the region of 0 to 10 W m^{-2} for all bands. Both the modelled and the normalized satellite data show a trend of decreasing radiance values across the reef top from pixel numbers 1 to 20. With the knowledge that submergence depth is constant across the first 17 pixels of the study area (figure 4), this suggests that the geomorphological and ecological zonation that exists on the reef top due to such factors as gradients in wave exposure, is represented by a decrease in radiance value from the shoreward to the seaward side. There is a pronounced drop in radiance in TM bands 2 and 3 (figure 8B and C respectively) between pixel numbers 17 and 20, which can be attributed to the rapid increase in water depth associated with crossing the reef break and the onset of the reef slope.

3. Discussion

3.1. Ground verification methodology

Published studies on coral reefs and associated sediments using satellite images were only partly successful in separating bottom types (Smith 1975, Kuchler *et al.* 1986, Luckovich *et al.* 1993, Peddle *et al.* 1995, Maritorena 1996, Maritorena and Guillocheau 1996, Matsunaga and Kayanne 1997, Borstad *et al.* 1997a, b). The best comparison study to that of the project was carried out by Luckovich *et al.* (1993) in the Dominican Republic. In general, several factors can be suggested to explain the limited success in discriminating bottom type categories with characteristic radiance values: (1) insufficient resolution and quantification of substrate mapping; (2) mapping of dominant rather than all species characteristic of bottom types; (3) changes in substrate coverage between acquisition of satellite image and survey (Michalek *et al.* 1991, Wagner *et al.* 1991); (4) the effect of variable water depth on the radiance characteristics of bottom types.

It is obvious that the above factors greatly affect the quality of the calibration between remotely sensed radiance and actual bottom type distribution. In the study

carried out by Luckovich *et al.* (1993), most ground-truthed pixels were submerged under ~ 3 m of water, whereas in this project water depth on the reef top was 0.7 m and fairly constant (± 0.3 m). Evidence from Zainal *et al.* (1993) suggests that submergence can cause some habitats to become spectrally similar. In particular, classification becomes difficult between seagrass and deep water and between seagrass, corals and algae (i.e. optically dark habitats) in areas greater than 5 m depth; the problem was also reported by Ackleson and Klemas (1987) and Vousden (1986). It is important to have detailed bathymetric data and reliable knowledge of the tidal cycle of a study area, if satellite radiance values are to be used to interpret reef bottom types.

The following methods to address the interpretation of satellite imagery, and specifically the problem of bathymetry, are proposed for future research. In areas with constant bottom type, usually seaward of the reef wall in water depths of typically 10 to 25 m, bathymetry can be estimated from blue–green wavelengths and calibrated with depth soundings. Studies in the Bahamas and offshore Cuba, indicated a penetration of blue–green wavelengths in clear water up to 20 m (Gordon and Brown 1974, Lyzenga 1978, 1981, Paredes and Spero 1983, Clark *et al.* 1987, Philpot 1989, Harris and Kowalik 1994), which is also the critical depth for reef growth (Bosscher and Schlager 1992). Algorithms for water depth mapping in coastal areas using satellite imagery were developed by Lyzenga (1978) and Paredes and Spero (1983). Van Hengel and Spitzer (1991) stated that the reliability of the computed water depths depends to a considerable extent on the accuracy of the known water depth data used to calibrate the algorithms. In cases where accurate calibration data on the depth are not available, a method such as the one presented by Lyzenga (1978) can be used as an assessment of relative water depths. This method is based on an assumed linearity of the water depth with the first principle component of the logarithms of the detected signals within the spectral bands of the satellite sensors. The absolute water depths can then be computed through calibration, applying several reference points where the true depths are known (Van Hengel and Spitzer 1991). In shallow water areas, less than 10 m (dominant depositional environment) with sufficient bottom currents (larger than 0.5 m s^{-1} , e.g. Bahamas), ESA's (European Space Agency's) SAR imagery, calibrated by depth surroundings, could be used to estimate water depth. Recent investigations have shown that sea surface roughness, imaged by radar, is a function of the friction of the water column with the sea floor, and is a valid proxy for bathymetry with a resolution within 0.5 m and to a depth of 20 m (Valenzuela *et al.* 1983, Alpers and Hennings 1984, Manière and Jaubert 1985, Harris *et al.* 1986, Vogelzang 1989, 1997a, b, Calkoen *et al.* 1993, Cooper *et al.* 1994). In areas of both variable water depth and bottom type, that lack sufficient current, only depth soundings or accurate bathymetric maps can solve the interpretation of the satellite radiance values in terms of substrate coverage. If reef substrates are going to be classified over wide areas, such as along the extent of an image, the development of a linear slope model of submergence depth on the reef top would be invaluable. This would be used to correct for the difference in tidal heights encountered when considering a large stretch of coastline.

3.2. Optical model

The optical model (figure 8) shows deviations of up to 60 W m^{-2} in TM bands 1, 2 and 3 in the extreme shoreward area of the reef top when compared with the normalized satellite image. Such deviations are to be expected, considering the simple

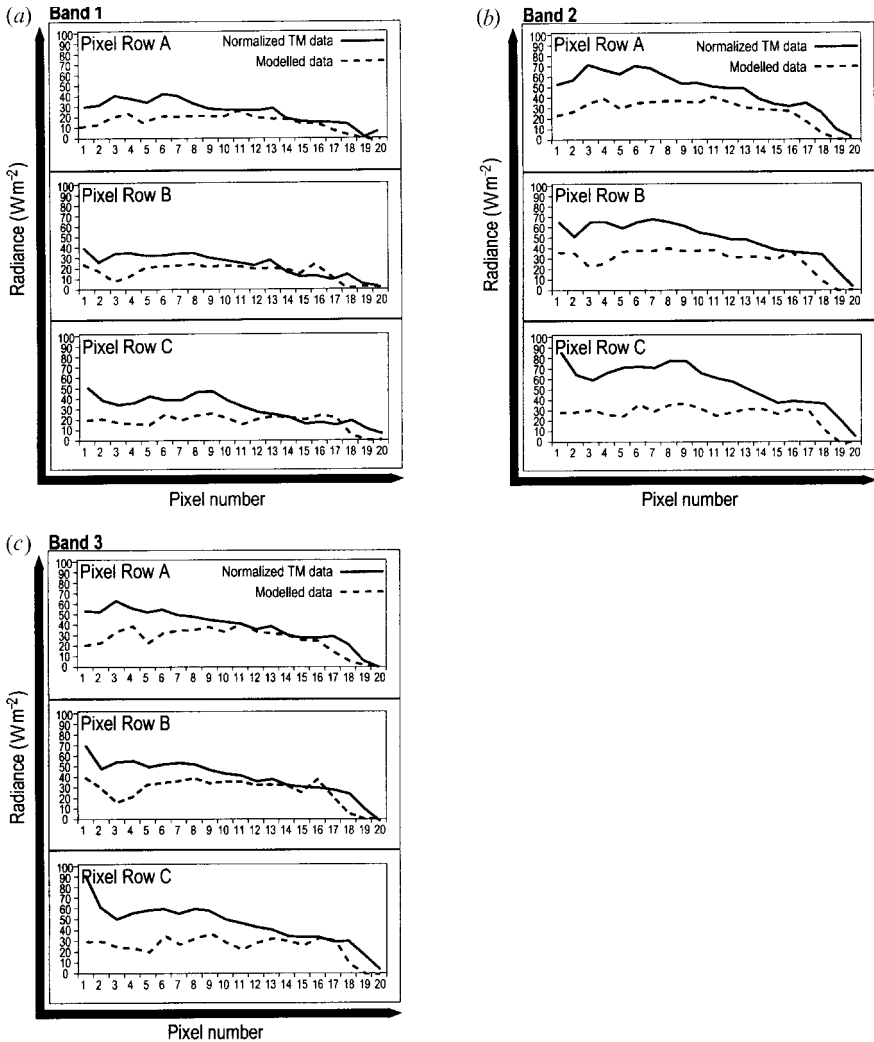


Figure 8. A series of graphs to show the difference between radiance values of the data modelled using literature spectral measurements and percentage cover of each of the twelve coverage classes, and those of the normalized satellite image. There is a plot for each pixel row across the reef top for Landsat TM bands 1–3 (*a*, *b* and *c* respectively).

algorithms used for atmospheric scattering, solar elevation angle, and water attenuation and the assumptions made when using radiance values from the literature. In addition, the satellite image is 14 years old and modifications in substrate distribution may well be expected over this period of time (Michalek *et al.* 1991, Wagner *et al.* 1991).

The optical response of reef substrates relies on a number of additional factors. The *in vitro* spectral albedo for macro-algae reflects the specific pigment composition of each taxonomic group (Maritorena and Guillocheau 1996). For example the green algae *Boodlea* sp. exhibits a prominent reflectance maximum at 550 nm (TM Band 2). This maximum corresponds to the green portion of the visible spectrum, which

is not strongly absorbed by chlorophyll. In addition the green algae shows distinct depressed reflectance values below 500 nm and around 675 nm (bands 1 and 3 respectively) which is characteristic of chlorophyll presence (Maritorena *et al.* 1994). The albedo of brown algae remains uniformly low throughout the spectrum with maximum values observed in the 570–650 nm domain (TM bands 2 and 3), resulting from the strong absorption by fucoxanthin and carotene (Maritorena and Guillocheau 1996). Since, in contrast to the green algae, brown algae is deprived of distinctive signatures within the spectral domain of penetrative radiation (< 580 nm), separation between these two algal types should be possible on a Landsat image. The red algae have a double peak at 600 nm (limit of TM band 2), and 650 nm (band 3). In band 1 albedos are above those of green and brown algae. The pattern is the result of the pigment phycobilin which depresses the albedo in the green part of the spectrum. Luckovich *et al.* (1993) stated that seagrass has a greater radiance than coral cover in Landsat bands 1, 2 and 3, although the mean radiance of seagrass and coral reef did not differ significantly in any band after analysis of variance and multivariate analysis of variance.

The albedo of highly reflective calcium carbonate debris is high, but dependent on submergence depth (Maritorena and Guillocheau 1996). When sampled in emerged zones, and therefore free of microphytobenthic organisms, such as cyanobacteria and diatoms, the albedo follows a smooth increase from short towards long wavelengths (i.e. increase from bands 1 to 4). Alternatively, once submerged the associated microphytobenthos would have a marked effect on the albedo. Despite this, Maritorena (1994) showed that a sandy bottom as deep as 15 m has a distinct signature that gives rise to reflectance values double that of R_{∞} (i.e. reflectance of the infinitely deep ocean). The data from the reefs of French Polynesia indicated that the reflectance of coral sand when measured at zero depth is greatest from 400–600 nm (bands 1 and 2), with increasing depth serving as to decrease reflectance above 600 nm (band 3). The work of Armstrong (1993) and Maritorena and Guillocheau (1996) showed carbonate sand to have a higher albedo than any seagrass or algal substrate in Landsat bands 1, 2 and 3. Armstrong (1993) demonstrated that at < 710 nm, the albedo of seagrass exceeds that of sand: this was not observed in any algae by Maritorena and Guillocheau (1996). In the work carried out by Luckovich *et al.* (1993) in the Dominican Republic, sand had significantly greater radiance than seagrass or coral in Landsat Band 1, resulting from small-scale patchiness. They stated that sand areas could be mapped efficiently using Landsat TM.

All of the at-sensor radiance values of the bottom substrates increase in the near infrared domain, however, the extreme attenuation of infrared wavelengths in water precludes their use in substrate detection using Landsat data. With the exception of submergence depth, it appears that the dominant factor controlling the predictability of a cluster's composition is its standard deviation. Clusters with a high standard deviation require the addition of ground verified field data in order to identify the bottom substrates that each pixel contains, and therefore the mixture of bottom types that each cluster represents. This suggests that Landsat imagery is sufficiently sensitive to discriminate between seagrass and other types of green algae as represented in the wide spread of radiance values around the pure green algae pixel. If this is the case then Landsat TM has much wider applications to the mapping of reef substrates than have been reported in the literature. When used with the appropriate cluster analysis techniques calibrated by *in situ* measurements Landsat TM can be sensitive enough to distinguish between different types of optically similar substrates,

such as between green algae and seagrass, and between brown algae and algal mats. Identification of different density substrates might also be possible, but given the heterogeneous nature of the reef top this is hard to verify because it is difficult to find pixels containing only one bottom type at constant density. The addition of the field data has also reaffirmed that bispectral and principal component techniques both have the ability to resolve satellite radiance values into clusters. Although both techniques yield the same number of clusters, the type of clusters differ between components and bispectral plots. Therefore the use of both techniques is advisable if the optimum amount of information is to be drawn from the data. Despite the fact that the analytical techniques have been successful when applied to the image of the project, we cannot conclude that the techniques could be expanded to estimate reef coverage over large areas without repetition of the study in another region using different images.

4. Conclusions

In the absence of a training set of ground-truth data, it was found that by applying bispectral and principal components plots of satellite radiance, pixels corresponding to sand and deep water could be recognized. The addition of pure pixels from the ground-truth data was used to characterize the clusters produced by the bispectral and principle components plots, 14 bottom type categories were defined, of which nine were immediately distinguishable from the training set. The field record then provided a mean substrate coverage for each cluster, with the result that the cluster categories were found to be composed of a mixture of various substrate densities with contamination from optically similar bottom types. The clusters which remained unclassified after the addition of pure pixel end members consisted of green and brown algae mixtures with contamination from seagrass, as predicted by their position on the bispectral and principal components plots.

The basis for an optical model to simulate the radiance of ground-truth data was then developed, which can benefit from the addition of a more stringent method of atmospheric correction and more advanced algorithm to simulate the attenuation of radiance in the visible band by water. A fundamental weakness of the model is the lack of accepted spectral at-surface radiance values for different substrates in the literature. This confirms that the use of a portable spectroradiometer which can measure at-surface radiance values in the visible and near-infrared (analogous to the range of the first four Landsat TM bands), or spectral signatures from a dedicated library of reef substrate optics, would provide invaluable data that could be incorporated into an improved optical model. Another weakness that could be resolved is the problem of varying submergence depth. In shallow areas with constant water depth, bathymetry can be assumed constant. In areas with sufficient current, synthetic aperture radar (SAR) data can be used as a proxy for bottom topography. In areas with constant bottom type, variable water depth and insufficient current, blue and green light absorption is a means for estimating bathymetry using Landsat TM imagery. Where both bathymetry and substrate vary, depth soundings or accurate bathymetric maps are needed. With these modifications, the optical model holds the potential to be implemented as a valuable predictive tool in order to simulate the upwelling radiance of different bottom types.

We view this research as a valuable preparatory step for reef mapping from other moderate resolution satellites such as Landsat 7 which was launched successfully in

April 1999. Unlike the previous Landsat satellites, Landsat 7 offers a spatial resolution of 15 m provided by an additional panchromatic channel. IRS, the Indian Remote Sensing Satellite program covers the green, red and near infrared portion of the spectrum with a spatial resolution of 23.5 m, resampled to 20 m. The successful launch of ASTER (Advanced Spaceborne Thermal Emission and Reflection Radiometer) was accomplished in December 1999. ASTER provides a ground resolution of 15 m in the visible and near infrared portion of the spectrum. The instrument will become extremely valuable for the continued effort to develop techniques whereby remote sensing can be used as a tool to detect reef substrates, when global data coverage is achieved in the near future.

Acknowledgments

We thank Hossam Helmy of Red Sea Diving Safari's for his hospitality and local support. Karen van Opstal is warmly thanked for sharing her views and invaluable expertise with us above and below the Red Sea water surface. Wolfgang Schlager, Freek van der Meer (ITC, Netherlands) and Ted Milton (University of Southampton, UK) are acknowledged for continuous support and discussions. Additional funding was provided through the Industrial Associates Program of the Sedimentology Group at the Vrije Universiteit, Amsterdam.

References

- ACKLESON, S. G., and KLEMAS, V., 1987, Remote sensing of submerged aquatic vegetation in lower Chesapeake Bay: a comparison of Landsat MSS to TM imagery. *Remote Sensing of Environment*, **22**, 235–248.
- ALPERS, W., and HENNINGS, I., 1984, A theory for imaging mechanism of underwater bottom topography by real and synthetic aperture radar. *Journal of Geophysical Research*, **89**, 10 529–10 546.
- ARMSTRONG, R. A., 1993, Remote sensing of submerged vegetation canopies for biomass estimation. *International Journal of Remote Sensing*, **14**, 621–627.
- BERGER, W. H., 1982, Increased carbon dioxide in the atmosphere during deglaciation: the coral reef hypothesis. *Naturwissenschaften*, **69**, 87–88.
- BORSTAD, G., BROWN, L., CROSS, W., NALLEE, M., and WAINWRIGHT, P., 1997a, Towards a management plan for a tropical reef-lagoonal system using airborne multispectral imaging and GIS. *Proceedings of the Fourth International Conference on Remote Sensing for Marine and Coastal Environments, Orlando, Florida, 17–19 March 1997* (Ann Arbor: Environmental Research Institute of Michigan), pp. 605–610.
- BORSTAD, G., LEE, E., and BROWN, L., 1997b, Mapping a Texas coastal lagoon with airborne multispectral imaging. *Proceedings of the Fourth International Conference on Remote Sensing for Marine and Coastal Environments, Orlando, Florida, 17–19 March 1997* (Ann Arbor: Environmental Research Institute of Michigan), pp. 565–571.
- BOSSCHER, H., and SCHLAGER, W., 1992, Computer simulation of reef growth. *Sedimentology*, **39**, 503–512.
- CALKOEN, C. J., KOOL, M. W. A., VAN DER HESSELMANS, G. H. F. M., and WENSINK, G. J., 1993, The imaging of sea bottom topography with polarimetric P-, L-, and C-band SAR. Report BCRS project 2.1/AO-02. Netherlands Remote Sensing Board, Delft.
- CLARK, R. K., FAY, T. H., and WALKER, C. L., 1987, Bathymetry calculations with LANDSAT-4-TM imagery under a generalised ratio assumption. *Applied Optics*, **26**, 4036–4038.
- COOPER, A. L., CHUBB, S. R., ASKARI, F., VALENZUELA, G. R., BENNET, J. R., and KELLER, W. C., 1994, Radar surface signatures for the two-dimensional tidal circulation over Phelps Bank, Nantucket Shoals: a comparison between theory and experiment. *Journal of Geophysical Research*, **99**, 7865–7883.
- GLYNN, P. W., 1991, Coral reef bleaching in the 1980s and possible connections with global warming. *Trends in Ecology and Evolution*, **6**, 175–179.

- GORDON, H. R., and BROWN, O. B., 1974, Influence of bottom depth and albedo on the diffuse reflectance of a flat homogeneous ocean. *Applied Optics*, **13**, 2153–2158.
- GRIGG, R. W., and DOLLAR, S. J., 1990, Natural and anthropogenic disturbance on coral reefs. In *Coral Reefs*, edited by Z. Dubinsky (New York: Elsevier), pp. 439–452.
- HALLOCK, P., and SCHLAGER, W., 1986, Nutrient excess and the demise of coral reefs and carbonate platforms. *Palaios*, **1**, 369–398.
- HARRIS, P. M., and KOWALIK, W. S., 1994, Satellite images of carbonate depositional settings. Examples of reservoir- and exploration-scale geologic facies variation. (Tulsa: The American Association of Petroleum Geologists).
- HARRIS, P. T., ASHLEY, G. M., COLLINS, M. B., and JANES, A. E., 1986, Topographic features of the Bristol Channel sea-bed: a comparison of SEASAT (synthetic aperture radar) and side-scan sonar images. *International Journal of Remote Sensing*, **7**, 119–136.
- HOLDEN, H., and LE DREW, E., 1997, Spectral Discrimination of bleached and healthy submerged corals based on principal components analysis. *Proceedings of the Fourth International Conference on Remote Sensing for Marine and Coastal Environments, Orlando, Florida, 17–19 March, 1997* (Ann Arbor: Environmental Research Institute of Michigan), pp. 177–186.
- KUCHLER, D. A., JUPP, D. L. B., VAN R. CLASSEN, D. B., and BOUR, W., 1986, Coral reef remote sensing applications. *Geocarto International*, **4**, 3–15.
- LEAVITT, B. C., and PAYTON, S. L., 1996, Integrating global positioning systems with satellite remote sensing: Avoiding major pitfalls. *Proceedings of the Annual Meeting, IEEE International Geoscience and Remote Sensing Society, Lincoln, Nebraska, 4–8 August 1996* (Piscataway, NJ: Institute of Electrical and Electronics Engineers), pp. 2273–2275.
- LUCKOVICH, J. J., WAGNER, T. W., MICHALEK, J. L., and STOFFLE, R. W., 1993, Discrimination of coral reefs, seagrass meadows, and sand bottom types from space—A Dominican Republic case study. *Photogrammetric Engineering and Remote Sensing*, **59**, 358–389.
- LYZENGA, D. R., 1978, Passive remote sensing techniques for mapping water depth and bottom features. *Applied Optics*, **17**, 379–383.
- LYZENGA, D. R., 1981, Remote sensing of bottom reflectance and water attenuation parameters in shallow waters using aircraft and Landsat data. *International Journal of Remote Sensing*, **2**, 71–82.
- MANIÈRE, R., and JAUBERT, J., 1985, Traitements d'image et cartographie de récifs coralliens en Mer Rouge (Golfe d'Aqaba). *Oceanologica Acta*, **8**, 371–381.
- MARITORENA, S., 1996, Remote sensing of the water attenuation in coral reefs: a case study in French Polynesia. *International Journal of Remote Sensing*, **17**, 155–166.
- MARITORENA, S., and GUILLOCHEAU, N., 1996, Optical properties of water and spectral light absorption by living and non-living particles and by yellow substances in coral reef water of French Polynesia. *Marine Ecology Progress Series*, **131**, 245–255.
- MARITORENA, S., MOREL, A., and GENTILI, B., 1994, Diffuse reflectance of oceanic shallow waters: Influence of water depth and bottom albedo. *Limnology and Oceanography*, **39**, 1689–1703.
- MATSUNAGA, T., and KAYANNE, H., 1997, Observations of coral reefs on Ishigaki Island, Japan, using Landsat TM images and aerial photographs. *Proceedings of the Fourth International Conference on Remote Sensing for Marine and Coastal Environments, Orlando, Florida, 17–19 March 1997* (Ann Arbor: Environmental Research Institute of Michigan), pp. 657–666.
- MAUL, G. A., 1985, *Introduction to Satellite Oceanography* (Dordrecht: Martinus Nijhoff Publishers).
- MICHALEK, J. L., CHRISTY, J. J., WOOD, L., and FULKERSON, S. A., 1991, Water depth extraction from satellite data with environmental and engineering applications. *Proceedings of the Eighth Thematic Conference on Geologic Remote Sensing, Denver, Colorado, 29 April–2 May 1991* (Ann Arbor: Environmental Research Institute of Michigan), pp. 141–162.
- MILLIMAN, J. D., and DROXLER, A. W., 1996, Neritic and pelagic carbonate sedimentation in the marine environment: ignorance is not bliss. *Geologische Rundschau*, **85**, 496–504.
- PAREDES, J. M., and SPERO, R. E., 1983, Water depth mapping from passive remote sensing data under a generalised ratio assumption. *Applied Optics*, **22**, 1134–1135.

- PEDDLE, D. R., LE DREW, E. F., and HOLDEN, H. M., 1995, Spectral mixture analysis of coral reef abundance from satellite imagery and *in situ* ocean spectra, Savusavu Bay, Fiji. *Third ERIM Thematic Conference on Remote Sensing of Marine and Coastal Environments, Seattle, Washington, 18–20 September 1995* (Ann Arbor: Environmental Research Institute of Michigan), pp. 563–575.
- PHILPOT, W., 1989, Bathymetric mapping with passive multispectral imagery. *Applied Optics*, **28**, 1569–1574.
- RICHARDS, J. A., 1986, *Remote Sensing Digital Image Analysis, An Introduction* (Berlin: Springer-Verlag).
- RIEGAL, B., and PILLER, W. E., 1997, Distribution and environmental control of coral assemblages in Northern Safaga Bay (Red Sea, Egypt), *Facies*, **36**, 141–162.
- SMITH, V. E., 1975, Automated mapping and inventory of Great Barrier Reef Zonation with Landsat data. *IEEE Journal of Oceanic Engineering*, **1**, 775–779.
- SHIFRIN, K. S., 1988, *Physical Optics of Ocean Water* (New York: American Institute of Physics).
- SPINRAD, R. W., CARDER, K. L., and PERRY, M. J., 1994, *Ocean Optics* (Oxford: Oxford University Press).
- VAN HENGEL, W., and SPITZER, D., 1991, Multi-temporal water depth mapping by means of Landsat TM. *International Journal of Remote Sensing*, **12**, 703–712.
- VALENZUELA, G. R., CHEN, D. T., GARRET, W. D., and KAISER, J. A. C., 1983, Shallow water bottom topography from radar imagery. *Nature*, **303**, 687–689.
- VOGELZANG, J., 1989, The mapping of bottom topography with imaging radar: a comparison of the hydrodynamic modulation in some existing models. *International Journal of Remote Sensing*, **10**, 1503–1518.
- VOGELZANG, J., 1997a, Mapping submarine sand waves with multiband imaging radar—1. Model development and sensitivity analysis. *Journal of Geophysical Research*, **102**, 1163–1181.
- VOGELZANG, J., 1997b, Mapping submarine sand waves with multiband imaging radar—2. Experimental results and model comparison. *Journal of Geophysical Research*, **102**, 1183–1192.
- VOUSDEN, D. P., 1986, The Bahrain marine habitat survey. Project Report, 1, Environmental Protection Committee, State of Bahrain.
- WAGNER, T. W., MICHALEK, J. L., and LAURIN, R., 1991, *Satellite Monitoring of Coastal Marine Ecosystems: A Case Study From the Dominican Republic*. Pilot Projects Draft Report, Consortium for International Earth Science Information Network, University Centre, Michigan.
- ZAINAL, A. J. M., DALBY, D. H., and ROBINSON, I. S., 1993, Monitoring of marine ecological changes on the east coast of Bahrain with Landsat TM. *Photographic Engineering and Remote Sensing*, **59**, 415–421.